ISSN: 2319-8753

International Journal of Innovative Research in Science, Engineering and Technology

(An ISO 3297: 2007 Certified Organization)

Vol. 3, Issue 8, August 2014

A Study on the Sintering Of HAp Sputtering Target Material for Biomedical Applications

Byeong-Mo Kang[1], Hyun-Kuk Park[2], Jun-Ho Jang[2], Woon-Jo Jeong[3], Kyung-Ku Lee[4], Ik-Hyun Oh[2], Hoon-Sung Cho[5], Ho-Geun Ahn[6], and Yeong-Seog Lim[1]

Research Scholar and Professor, Department of Electronics and Computer Engineering, Chonnam National University, Gwangju, South Korea[1]

Research Scholar, Korea Institute of Industrial Technology (KITECH), Gwangju, South Korea[2]

Research Scholar, OT&T Inc., Gwangju, South Korea[3]

Research Scholar, R&D Center for Ti and Special Alloys, Gwangju, South Korea [4]

Professor, School of Materials Science and Engineering, Chonnam National University, Gwangju, South Korea[5]

Professor, Department of Chemical Engineering, Sunchon National University, Suncheon, Jeonnam, South Korea[6]

ABSTRACT: Using the spark plasma sintering (SPS) method, hydroxyapatite (HAp) material was densified using a hydroxyapatite powder (RND Korea, 45 ㎛, purity 98 +%). The HAp was nearly completely dense with a relative density of up to 97 % after the simultaneous application of 60 MPa of pressure and about 30 minutes of electric current without significant change in the grain size. The average grain size of HAp that was produced through SPS was approximately 13.2 ㎛. The hardness and fracture toughness of the HAp sintered-body at 1200 °C were 253 ± 0.5 kg/mm^2 and 0.48 ± 0.02 MPam$^{1/2}$.

KEYWORDS: Hydroxyapatite, Spark Plasma Sintering Process, Hardness, Fracture toughness, Rapid Sintering.

I. INTRODUCTION

Titanium and titanium alloy have been commonly used for medial implantations because of their excellent bio-compatibility. However, its lack of bioactivity slows osteogenesis and results in long recovery time and weak binding affinity between bone and the surface of an implant. Therefore there have been numerous studies for improving osseintegration by physical and chemical modifications of the surface [1] or compositional or morphological changes of the implant [2]. Especially, technology of coating hydroxyapatite (HAp), among the leading bioactive materials, has been steadily developed for reducing treatment time by stimulating osteogenesis and increasing interfacial binding of the implant since 1990s [3]-[4]. In this study, HAp sputtering target material for bioactive coating having close-packed structure and homogeneity was synthesized using spark plasma sintering (SPS) and its physical and mechanical characteristics was evaluated.

II. RELATED WORK

HAp or other calcium phosphates are generally applied to improve bioactivity of metal implants as a coating. Because of the chemical and crystallographic similarities with the inorganic components of human bones, HAp or calcium phosphate layers lead to direct bonding or earlier stabilization of implants with the surrounding bones or tissues [5]-[6]. Also, the bond strength of a coating layer with the metal substrate is a very important factor. If the layer is separated from the implant during actual applications in human body, the detached fragments have very adverse effects on the implant or the tissue surrounding it [7]. Another important property that the coating layer should possess is a low dissolution rate in aqueous solutions. If the dissolution rate is faster than bone growth or implants stabilization, the

DOI: 10.15680/IJIRSET.2014.0308003

ISSN: 2319-8753

International Journal of Innovative Research in Science, Engineering and Technology

(An ISO 3297: 2007 Certified Organization)

Vol. 3, Issue 8, August 2014

coating is useless. The dissolution rate of crystalline HAp has been observed to be very low, while that of the amorphous phase was considerably high.

Among the HAp coating techniques, plasma spray method is the most famous process for manufacturing commercial implants because of its simplicity and versatility [3]. However it had several drawbacks, such as, chemical and structural disconformity of HAp coating layer, weak binding strength of HAp coating layer, and degradation and absorption of HAp into the microorganism of the human body [8]. Regardless of the coating methodology, amorphous layers are generally formed on metal substrates, which have a high dissolution rate in aqueous solutions. Therefore, the layers are subsequently heat-treated at approximately 600 °C in order to convert the amorphous phase into a crystalline phase [9]. However, the heat treatment causes cracks in the layer due to a thermal expansion mismatch between the coated layer and the metal substrate. This leads to a severe reduction in bond strength [10]. Thereby there has been several approaches of physical coating technologies for HAp coating, for example, ion beam sputtering method, rf sputtering method, and pulsed laser deposition [11]-[13].

Spark plasma sintering (SPS) can be employed at low temperatures and in short duration of time, compared to the typical methods, because the powder surface is activated by applying a high-voltage pulse current between gaps in the powder. One advantage of this process is that a compact microstructure with a high density and tiny pores can be fabricated. Recently, SPS has been widely studied and applied to industry because of its advantages. Densification by SPS is extremely fast compared to conventional sintering methods in which an external pressure is applied, such as hot pressing (HP) or hot isostatic pressing (HIP). Thus, the sintering temperatures can be lower, which limits the grain growth [14]-[16]. So in view of the demands of high quality, fast and mass products manufacturing of HAp sputtering target, the objective of this work is to study the characteristics of HAp sintered-body fabricated by SPS.

III. EXPERIMENTAL DETAILS

Hydroxyapatite powder (RND Korea, 45 ㎛, purity 98 +%) was used as the starting materials. Fig. 1 shows the micro-structure of the initial powder using scanning electron microscopy (SEM). The powders are composed of hexagonal crystals and conglomerated. Particle size was analyzed as shown in Fig. 2 using a particle size analyzer (Malvern, Mastersizer 2000E) and ranged between 0.5 ~ 100 μm with 10 μm in average.

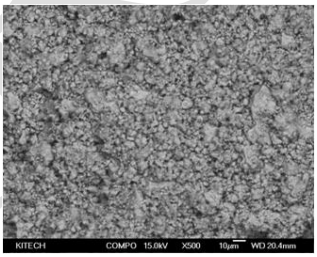

Fig. 1 Micro-structure of the initial HAp powder (RND Korea, 45 ㎛, purity 98 +%) using scanning electron microscopy

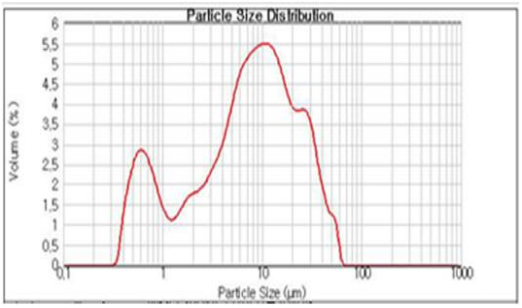

Fig. 2 Particle size analysis of HAp powder using a particle size analyzer (Malvern, Mastersizer 2000E)

DOI: 10.15680/IJIRSET.2014.0308003

ISSN: 2319-8753

International Journal of Innovative Research in Science, Engineering and Technology

(An ISO 3297: 2007 Certified Organization)

Vol. 3, Issue 8, August 2014

Analysis of X-ray diffraction (XRD) pattern of HAp powder reveals that only $Ca_{10}(PO4)_6(OH)_2$ phase was found and no secondary phase was detected. It also indexed HCP crystals and semi-stable TCP phases of the powder (Fig. 3). XRD data was used for granularity, using Stokes and Wilson's formula as follows [17]:

$$B = b_d + b_e = k\lambda / (d\cos\theta) + 4\varepsilon\tan\theta$$

where, b is the full width at half-maximum (FWHM) of the diffraction peak after the instrumental correction; b_d and b_e are the FWHM for a small grain size and internal strain, respectively; k is a constant (with a value of 0.9); λ is the wavelength of the X-ray radiation; d and ε are the grain size and the internal strain, respectively; and θ is the Bragg angle. The average grain size using XRD patterns is 13.5 μm, which is similar to the result by the particle size analyzer.

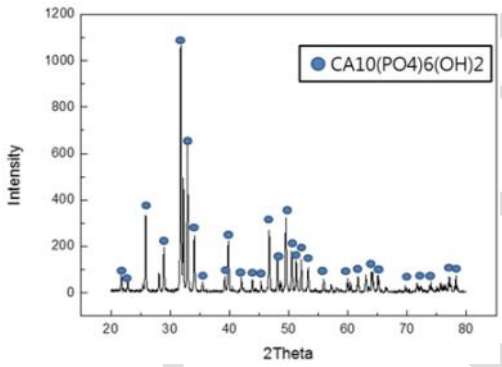

Fig. 3 Analysis of X-ray diffraction (XRD) pattern of HAp powder

Hydroxyapatitie powders were placed in a graphite die (outside diameter, 30 mm; inside diameter, 10 mm; height, 40 mm), and then placed into a rapid sintering system that was made by Sumitomo Coal Mining in Japan. A schematic diagram of this method is shown in Fig. 4. The SPS apparatus included a 25 V, 1000 A DC power supply (which provided a pulsed current for 12 ms with an off time of 2 ms through the sample and die) and a 10 ton uniaxial press. First, the system was evacuated, and a uniaxial pressure of 60 MPa was applied. Then, a DC current was activated and maintained until the densification rate was negligible, as indicated by the observed shrinkage of the sample. The sample shrinkage was measured in real time using a linear gauge for the vertical displacement. The temperature was measured using a pyrometer that was focused on the surface of the graphite die. Depending on the heating rate, the electrical and thermal conductivities of the compact, and its relative density, the temperature on the surface and in the center of the sample could differ. The heating rate was approximately 40 $Kminute^{-1}$ during this process. After the process was complete, the current was turned off, and the sample was allowed to cool to room temperature.

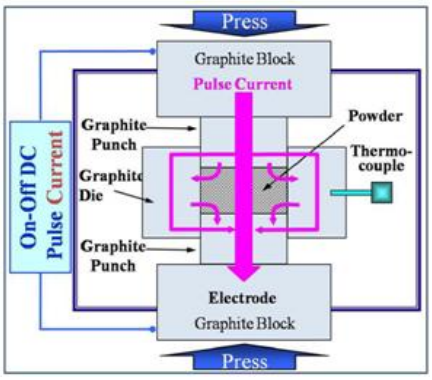

Fig. 4 Schematic diagram of experimental apparatus for spark plasma sintering included a 25 V, 1000 A DC power supply (which provided a pulsed current for 12 ms with an off time of 2 ms through the sample and die) and a 10 ton uniaxial press

DOI: 10.15680/IJIRSET.2014.0308003

ISSN: 2319-8753

International Journal of Innovative Research in Science, Engineering and Technology

(An ISO 3297: 2007 Certified Organization)

Vol. 3, Issue 8, August 2014

The entire densification process using the SPS technique consisted of four major control stages, including the chamber evacuation, pressure application, power application, and cool down. The four major sintering stages are schematically shown in Fig. 5. This process was carried out under a vacuum of 6 Pa. The relative densities of the sintered samples (Fig. 6) were measured using the Archimedes method. Microstructural information was obtained from the product samples, which were polished. The compositional and microstructural analyses of the products were carried out through X-ray diffraction (XRD) and field-emission scanning electron microscopy (FE-SEM). The micro-vickers hardness was measured by performing indentation tests at a load of 500 g and a dwell time of 15 s.

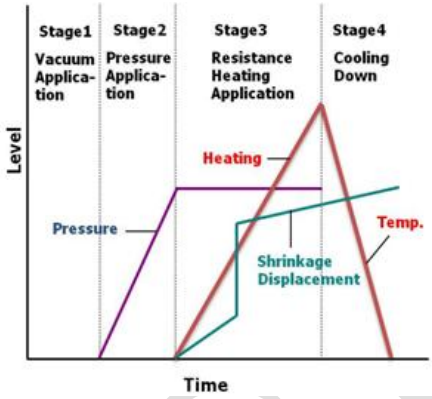

Fig. 5 Four major sintering stages and schematic representation of the temperature, pressure and shrinkage displacement profile during spark plasma sintering

Fig. 6 Fabricated HAp sintered-body using spark plasma sintering (10mmΦ x 2.5mm)

IV. RESULTS AND DISCUSSION

The variations of shrinkage displacement and temperature with heating time during the sintering are shown in Fig. 7. The shrinkage displacement was constantly decreased up to 950 °C and then rapidly increased after 950 °C. Expansion at early stage of the sintering might be induced by a high thermal expansion coefficient of HAp powder and a large difference between the thermal expansion coefficient of Ca and P. Fig. 8 showing the relative density as a function of the sintering temperature was obtained from the date of Fig. 7 including the changes of shrinkage length along with the sintering temperature. As the sintering temperature increased, there are abrupt changes of the relative density in the sintered pellets at 1100 °C and 1200 °C. It is possible that the variation of the relative density as a function of the temperature as shown in Fig. 8 were obtained by the following formula:

$$D_T = (L_f/L_T) \cdot D_f$$

where, D_T is the instantaneous relative density, L_f the final height, L_T the instantaneous height and D_f is the final relative density [18].

DOI: 10.15680/IJIRSET.2014.0308003

ISSN: 2319-8753

International Journal of Innovative Research in Science, Engineering and Technology

(An ISO 3297: 2007 Certified Organization)

Vol. 3, Issue 8, August 2014

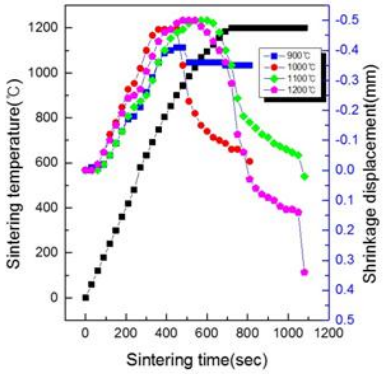

Fig. 7 Variations of temperature and shrinkage displacement with sintering time during spark plasma sintering

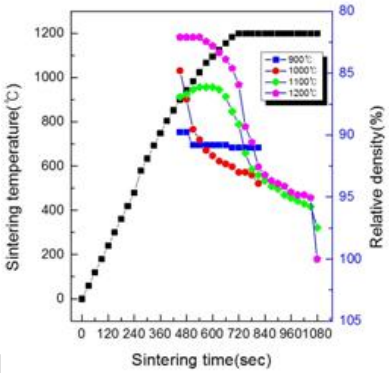

Fig. 8 Variations of temperature and relative density with sintering time during spark plasma sintering

Fig. 9 shows the XRD patterns of the sintered materials for different temperature. It shows that there is no secondary phase except $Ca_{10}(PO_4)_6(OH)_2$ same as in the initial powder. Average grain sizes and relative density were used by Stokes and Wilson's formula and Archimedes method.

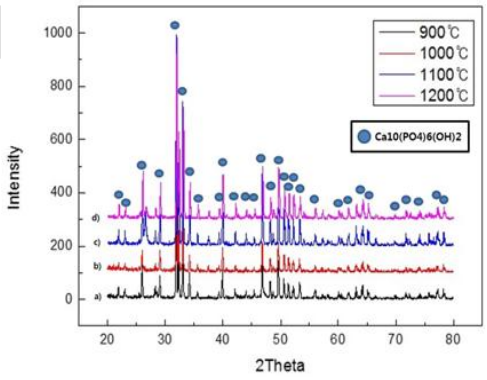

Fig. 9 XRD patterns of HAp sintered-body : a) 900°C, b) 1000°C, c) 1100°C, and d) 1200°C

Average grain sizes and relative density of HAp sintered-body were about 7.4, 7.5, 11.1 and 13.2 μm and 85, 86, 89 and 97 %, respectively (Fig. 10). It appears that the higher sintering temperature, the higher density the sintered HAp has, and finally, 97 % density was obtained at 1200 °C.

DOI: 10.15680/IJIRSET.2014.0308003

ISSN: 2319-8753

International Journal of Innovative Research in Science, Engineering and Technology

(An ISO 3297: 2007 Certified Organization)

Vol. 3, Issue 8, August 2014

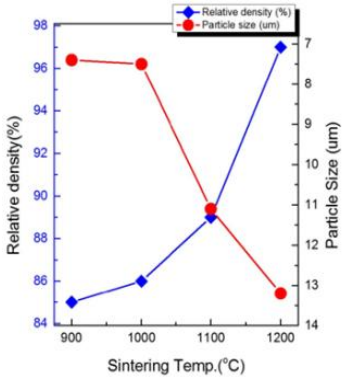

Fig. 10 Variations of temperature and relative density with particle size during spark plasma sintering

Fig. 11 shows the SEM images of the surfaces sintered at different temperatures. Porosities at the surface were reduced as the temperature increased and dense microstructure without porosities was observed at 1200 °C.

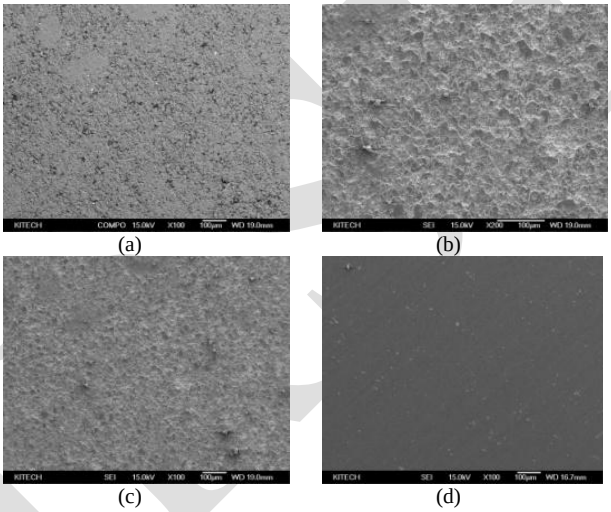

Fig. 11 FE-SEM images of the surfaces sintered at different temperatures: (a) 900°C, (b) 1000°C, (c) 1100°C, and (d) 1200°C

Table 1 gives the results of EDAX analysis and Fig. 12 shows that the ratio of calcium to phosphorus is about 1.907, 1.715, 1.612, and 1.645 from the sintered HAp at 900, 1000, 1100, and 1200 °C, respectively. It appears that the ratio was decreased as the temperature increased, however the numbers are all similar except one from 900 °C.

Table 1: Results of EDAX analysis sintered at different temperatures: (a) 900°C, (b) 1000°C, (c) 1100°C, and (d) 1200°C

	(a)		(b)		(c)		(d)	
Element	Wt.%	At.%	Wt.%	At.%	Wt.%	At.%	Wt.%	At.%
OK	46.00	65.96	29.83	49.01	39.01	59.02	36.94	58.00
PK	18.57	13.75	25.84	21.92	23.34	18.24	23.84	18.92
CaK	35.43	20.28	44.33	29.07	37.64	22.73	39.22	23.08
Matrix	Correction	ZAF	Correction	ZAF	Correction	ZAF	Correction	ZAF

DOI: 10.15680/IJIRSET.2014.0308003

ISSN: 2319-8753

International Journal of Innovative Research in Science, Engineering and Technology

(An ISO 3297: 2007 Certified Organization)

Vol. 3, Issue 8, August 2014

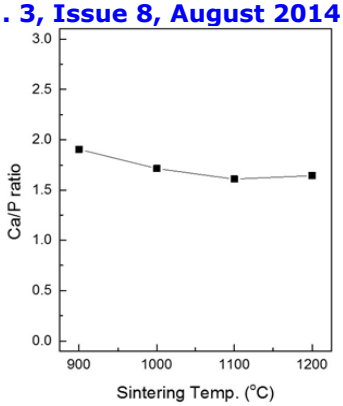

Fig. 12 Ca/P ratio of HAp sintered-body at different temperatures

The mechanical property of the sintered HAp was performed using the Vickers hardness measurements taken on the polished sections of the sintered HAp sintered-body using a 0.5 gf load (Fig. 13). The indentation produced median cracks that emanated from the corners of the indent. Length of radical cracks is related to the fracture toughness. Indentation fracture toughness was calculated using the Antis equation [19]:

$$K_{IC} = 0.016 \times (E/H)^{1/2} \times P/C^{3/2}$$

where E is Young's modulus of the sample, H is microhardness in GPa, P is the applied load, C is the half of the crack length, and K_{IC} is the indentation fracture toughness. The average microhardness values of HAp sintered at 1100 and 1200 °C were 221 and 253 kg/mm^2 and indentation fracture toughness was 0.43 and 0.48 MPam$^{1/2}$, respectively. Unfortunately, measurement of mechanical properties of HAp sintered at 900 and 1000 °C was failed because they were not fired at optimum.

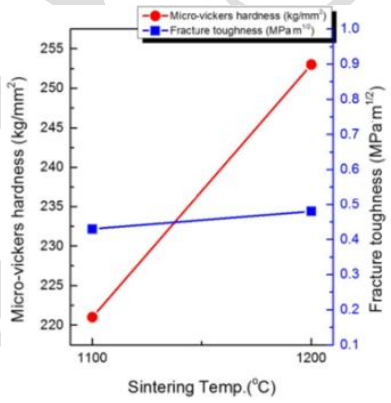

Fig. 13 Variations of temperature and Micro-Vickers hardness with fracture toughness during spark plasma sintering

V. CONCLUSION

HAp target sintered-body for vacuum deposition like rf magnetron sputtering was synthesized using SPS with different sintering temperatures. The relative density of the sintered HAp was increased as the sintering temperature increased and the HAp density sintered at 1200 °C was 97 % of theoretical density. With an increase in temperature, the average grain size also increased. The average grain size of sintered-body at 1200 °C was 13.2 μm, which means that the grain growth is limited from the average particle size of HAp powder, 10 μm and thereby dense microstructured HAp targets were produced. The hardness and fracture toughness of the HAp compacts sintered at 1200 °C were 253 ± 0.5 kg/mm^2 and 0.48 ± 0.02 MPam$^{1/2}$.

Acknowledgment: This research was financially supported by the INNOPOLIS Foundation (2013B012).

ISSN: 2319-8753

International Journal of Innovative Research in Science, Engineering and Technology

(An ISO 3297: 2007 Certified Organization)

Vol. 3, Issue 8, August 2014

REFERENCES

[1] Cochran D. L., Schenk R. K., Lussi A., Higginbottom F. L., and Buser D., "Bone response to Unloaded and Loaded Titanium Implants with a Sandblasted and Acid-Etched Surface : A Histometric Study in the Canine Mandible", J. Biomed. Mater. Res., Vol.40, No.1, pp.1-11, 1998.

[2] Okazaki K., Lee W. H., Kim D. K., and Kopczyk R. A., "Physical characteristics of Ti-6Al-4V implants fabricated by electrodischarge compaction", J. Biomed. Mater. Res., Vol.25, pp.1417-1429, 1991.

[3] Aoki H. and Li T., "Development and Clinical Studies of HA Coated Dental Implants using Various Techniques", J. Australian Ceramic Soc., Vol.47, pp.61-63, 2011.

[4] Catledge S. A., Fries M. D., Vohra Y. K., Lacefield W. R., Lemons J. E., Woodard S., and Venugopalan R., "Nanostructured Ceramics for Biomedical Implants", J. Nanosci. Nanotech., Vol.2, pp.293-312, 2002.

[5] Suchanek W. and Yoshimura M., "Processing and properties of hydroxyapatite-bases biomaterials for use as hard tissue replacement implants", J. Mater. Res., Vol.13, Issue 01, pp.94-117, 1998.

[6] LeGeros R. Z., "Biodegradation and bioresorption of calcium phosphate ceramics", Clinical Mater., Vol.14, Issue 1, pp.65-88, 1993.

[7] Wang S., Lacefield W.R., and Lemons J. E., "Interfacial shear strength and histology of plasma sprayed and sintered hydroxyapatite implants in vivo", Biomaterials, Vol.17, Issue 20, pp.1965-1970, 1996.

[8] Ito K., Nanba K., Nishida T., Sato H., and Murai S., "Comparison of Osseointegration Between Hydroxy -apatite Coated and Uncoated Threaded Titanium Dental Implants Placed into Surgically Created Bone Defect in Rabbit Tibia", J. Oral Sci., Vol.40, pp.37-41, 1998.

[9] Gross K. A., Gross V., and Berndt C. C., "Thermal analysis of amorphous phases in hydroxyapatite coatings", J. Am. Ceram. Soc., Vol.81, Issue 1, pp.106-112, 1998.

[10] Chen J., Tong W., Coa Y., Feng J., and Zhang X., "Effect of atmosphere on phase transformation in plasma sprayed hydroxyapatite coatings during heat treatment", J. Biomed. Mater. Res., Vol.34, pp.15-20, 1997.

[11] Lucas L. C., Lacefield W. R., Ong J. L., and Whitehead R. Y., "Calcium Phosphate Coatings for Medical and Dental Implants", Colloids Surf., Vol.77, pp.141-147, 1993.

[12] Ozeki K., Yuhta T., Fukui Y., and Aoki H., "Phase Composition of Sputtered Films from a Hydroxyapatite Target", Surf. Coat. Tech., Vol. 160, pp.54-61, 2002.

[13] Blind O., Klein L. H., Dailey B., and Jordan L., "Characterization of hydroxyapatite films obtained by pulsed-laser deposition on Ti and Ti-6Al-4V substrates", Dental Mater., Vol.21, Issue 11, pp.1017-1024, 2005.

[14] Orru R., Licheri R., Locci A. M., Cincotti A., and Cao G., "Consolidation/synthesis of materials by electric current activated/assisted sintering", Mater. Sci. Eng. R., Vol.63, pp.127-287, 2009.

[15] Reia J. and Chaim R., "Densification maps for spark plasma sintering of nanocrystalline MgO ceramics: Particle coarsening and grain growth effects", Mater. Sci. Eng.: A, Vol.491, pp.356-363, 2008.

[16] Chen W., Anselmi-Tamburini U., Garay J. E., Groza J. R., and Munir Z. A., "Fundamental investigations on the spark plasma sintering/ synthesis process : I. Effect of dc pulsing on reactivity", Mater. Sci. Eng.: A, Vol.394, pp.132-138, 2005.

[17] Zhang F. L., Wang C. Y., and Zhu M., "Nanostructured WC/Co composite powder prepared by high energy ball milling", Scripta Materialia, Vol.49, pp.1123-1128, 2003.

[18] Bernard-Granger G. and Guizard C., "Spark plasma sintering of a commercially available granulated zirconia powder: I. Sintering path and hypotheses about the mechanism(s) controlling densification", Acta Mater., Vol.55, pp.3493-3504, 2007.

[19] Anstis G. R., Chantikul P., Marshall D. B., and Lawn B. R., "A Critical Evaluation of Indentation Techniques for Measuring Fracture Toughness: I. Direct Crack Measurements", J. Am. Ceram. Soc., Vol.64, No.9, pp.533-538, 1981.